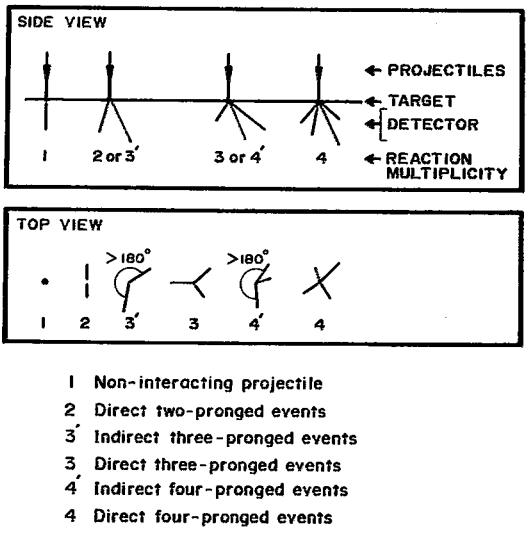

Fig. 1. Schematic representation of 2π-geometry technique using a mica solid state nuclear track detector. The reaction products after making damage trails are stopped in the mica, revealed with etching and observed with an optical microscope. Views of the events from the top of the detector as well as from one side are shown.

this work, it has shown that, for each three-pronged event, there exists at least one pair of nuclei whose relative velocity is consistent with the binary fission of an equilibrated nucleus. It is thus possible to establish that the reaction proceeds through a two-step process. In the first step, the projectile and target interchange mass and energy in such a way that one of the nuclei becomes unstable with respect to fission. However the time-lag between the dissociation of a composite system and the subsequent decay of a projectile-like or target-like nucleus is sufficiently large so that the statistical equilibrium is achieved by the decaying nucleus. The first-step of the reaction is most likely a deep-inelastic process, as evidenced by the large Total Kinetic Energy Loss (TKEL) while the second step is a normal binary fission. We have also determined the masses of final and intermediate reaction products. The isotropic relative-velocity distribution with respect to the in-plane angle suggests the absence of non-equilibrium or proximity effects.

2. EXPERIMENTAL PROCEDURE

The principle of 2π-geometry technique is shown in Fig. 1. The target material UF_4 was vacuum deposited on the surface of muscovite mica. The target thickness (T) was determined by weighing the mica before and after the deposition. The total target thickness of the four samples used was 4.7059 mg/cm^2. The samples were irradiated perpendicular to their surface with about 2×10^6 xenon projectile/cm^2, having 17.0 MeV/u energy, at the UNILAC (GSI), Darmstadt, Germany. The selected intensity of the beam gives a reasonable number of reaction events. The fluence (time-integrated flux) of the projectiles is chosen to be large enough that it yields as many reaction events with U^{238} present in the UF_4 as possible without causing overlapping of neighbouring events.

After the irradiation, the target material was removed by dissolving with HNO_3 and mica samples were etched with 40% H_2F_2 at room temperature for 80 min. After cleaning and drying the detectors, they were scanned under an optical microscope at a magnification of about $400\times$. A total area of 51.52 cm^2 was scanned in which we observed a number of binary as well as multi-prong events which are recorded in Table 1.

Among the 505 binary events observed we could bifurcate events 111 and 404 as elastic and inelastic events, respectively. This bifurcation was performed by comparing the observed track parameters (track lengths and their angles with respect to the beam direction) of each individual event with those calculated by the theoretical elastic scattering formula. The events sorted out on the basis of this criterion were further examined to see whether they corresponded to the masses of the projectile and target and to the incident projectile's energy (Baluch *et al.*, 1996). The 404 inelastic events were also analysed separately and the results will be presented elsewhere. Similarly, the observed multi-prong events could be grouped into two distinct types, namely, "direct" and "indirect" events. In an indirect event, the largest angle between any two neighbouring tracks in the plane of observation is larger than 180°. In this case it is assumed that at least one more fragment must have been emitted but is not registered due to one of the following reasons: either it was too light to be detected (below the detector threshold), it was emitted in the backward 2π-solid angle or entered the detector surface with an angle smaller than the critical angle of the detector (Khan and Durrani, 1972). The indirect events cannot be analysed kinematically, but they are taken into account for the determination of cross sections.

Table 1. Statistics of events of various multiplicities. E and IE stand for elastic and inelastic events whereas D and ID stand for direct and indirect events

Binary			Three-prong			Four-prong		
E	IE	Total	D	ID	Total	D	ID	Total
111	404	515	93	178	271	6	14	20

3. METHOD OF DATA ANALYSIS

As far as the direct multi-prong events are concerned, the masses and energies of these fragments were determined by using the correlated three-dimensional coordinates of their tracks in conjunction with the equations for the conservation of momentum and range–energy relations of the ions registered in the detector.

In fact, each track is like a well-defined vector in space and, accordingly, each of the two-, three- or four-prong events is characterized by its correlated two, three or four track vectors in the exit channel. Using the requirement of the conservation of momentum the correlated fragment masses m_i and velocities V_i from an individual multi-prong event can be calculated on the basis of the measured correlated track lengths l_i and track directions e_i. For this purpose we solved the equations event by event:

$$\sum_{i=1}^{N} m_i V_i(l_i,m_i)\cdot\hat{e}_i = \hat{P}_{in} \qquad (1)$$

where $\hat{P}_{in}$ denotes the incident (linear) momentum of the projectile, $V(l,m)$ is an empirical velocity–range relation and N (= 2, 3 or 4) is the multiplicity of the event.

Obviously, there is no simple relationship between length and fragment mass of an individual track in a multi-prong event. The balance of momenta of all the fragments involved determines the mass which has to be associated with a given track of a given direction and length. A polynomial of second order in mass and fourth order in range was used for the relation between experimental track lengths, velocities and masses (Gottschalk *et al.*, 1983):

$$V_i(l_i,m_i) = \sum_{\mu=0}^{2}\sum_{\nu=0}^{4} c_{\mu\nu} m_i^{\mu} l_i^{\nu} \qquad (2)$$

To a first approximation, the track length l_i is a measure of the specific energy (velocity) of the ith fragment. In general, the track length of an energetic particle depends on its velocity and mass. Substituting equation (2) into equation (1) one can solve it using the given coefficients $c_{\mu\nu}$ and e_i, knowing P_{in} from the mass and energy of the incoming projectile. Equations (1) and (2) are solved by standard numerical methods. The resulting masses are substituted back into $V_i(l_i,m_i)$ and the velocities are obtained in a second step. For this purpose a computer code, PRONGY (Gottschalk *et al.*, 1983), has been employed.

The coefficients of the polynomial were obtained by an internal calibration procedure, i.e. by using the track lengths of the elastic binary events in equation (2). The coefficients obtained were iteratively checked by solving equations (1) and (2) for elastic two-prong events until they yielded the masses of the projectile and target along with zero kinetic energy loss (Baluch *et al.*, 1996). The coefficients were further checked to see whether the total mass in three-prong events is equal to the sum of the projectile and target mass. The list of the best coefficients deduced from the internal calibration of the reaction is given in Table 2. We have neglected the isotropic emission of light particles as these make no essential change in the kinematical spectrometry of heavy reaction products (Gottschalk *et al.*, 1983).

Table 2. List of 15 coefficients ($c_{\mu\nu}$) used in equation (2)

$c_{\mu\nu}$	$\mu = 0$	$\mu = 1$	$\mu = 2$
$\nu = 0$	2.166×10^{-1}	-3.223×10^{-3}	9.600×10^{-6}
$\nu = 1$	-8.869×10^{-3}	7.298×10^{-4}	-2.238×10^{-6}
$\nu = 2$	1.953×10^{-3}	-4.905×10^{-5}	1.461×10^{-7}
$\nu = 3$	-6.825×10^{-5}	1.366×10^{-6}	-3.917×10^{-9}
$\nu = 4$	6.988×10^{-7}	-1.271×10^{-8}	3.526×10^{-11}

4. RESULTS AND DISCUSSION

Following the procedure mentioned above, we could analyse 44 out of 93 measured three-prong events. The rest of the events did not yield any solution of the above-mentioned equations. The origin of this failure could be traced to the observational difficulties leading to inaccurate measurements. For each analysed event a unique set of three masses could be obtained corresponding to the three correlated tracks.

4.1. *Relative velocities and masses of the fragments in the exit channel*

Once the masses have been assigned to the individual tracks, the velocities can be determined directly from equation (2). Thereby, in each multi-prong event, it becomes possible to determine the relative velocity between each pair of two correlated fragments. Obviously, we observe three different relative velocities between three pairs of correlated fragments. Theoretically, the relative velocity of any two fission fragments of a multi-prong event can be calculated using the following expression:

$$V_{ij} = [2Q_{ij}(m_i + m_j)/m_i m_j]^{1/2} \qquad (3)$$

where m_i, m_j are the masses of the fission fragments and $Q_{ij} \approx 0.124\ Z^2/A^{1/3} \approx 0.02A^{5/3}$ for a fragment of charge Z and mass number A.

The average value of V_{ij} for fission fragments is expected to be 2.4 ± 0.4 cm/ns. We have observed that one of the relative velocities in all the analysed three-prong events corresponds to the value expected from the fission process and is shown in Fig. 2. The other two values of relative velocities were far away from this value.

Hence, it is clear from all the analysed three-prong events that the reaction mechanism involved in this multiplicity is a sequential fission process. Moreover,

the values of the relative velocities enable us to identify the fission fragments produced in the second step of the reaction and are shown in Fig. 3, where m_1 and m_2 represent the lighter and heavier fission fragments and m_3 shows the mass distribution of the unfissioned fragment. The distrubutions have been fitted by Gaussians with mean values and standard deviations shown in the figures.

4.2. *Intermediate masses and mutual mass transfer*

Using the knowledge of relative velocity, we could reconstruct the first step of the reaction and therefore could determine pre-fission masses, event-by-event, by adding the observed masses of the fission fragments. Figure 4 represents the pre-fission mass distribution of all the analysed three-prong events in the first reaction step. Again, the Gaussians have been fitted to the experimental data with the values obtained from the arithmetic means and standard deviations.

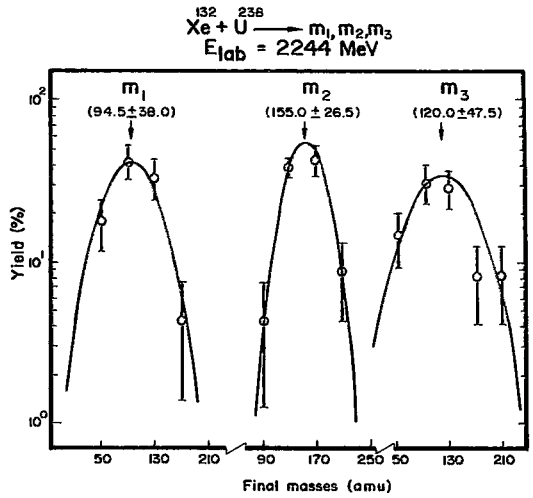

Fig. 3. Distribution of the final fragment masses integrated over all angles and energies in the case of three-prong events. Gaussians have been fitted with the arithmetic means and standard deviations.

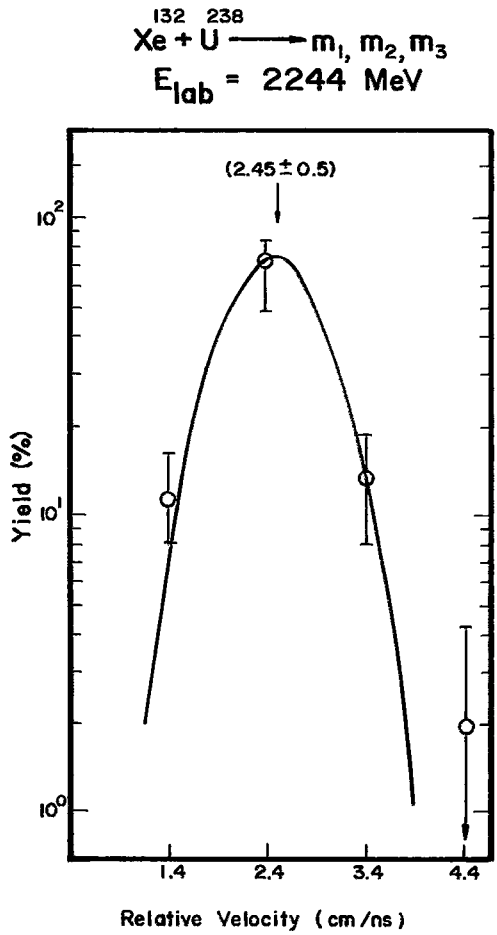

Fig. 2. Distribution of relative velocities of one pair of fragments for each of the 44 three-prong events. A Gaussian is fitted to the experimental points with (2.45 ± 0.5) cm/ns which are also the arithmetic mean and standard deviation.

After reconstruction of the masses, we are now in a position to determine the mass transfer in the first reaction step by taking the difference of mass between the projectile/target and intermediate fragments ($\Delta m = (132 - m_k)$ or $(238 - m_{ij})$. Hence an average of 12 amu mass transfer has been observed in the first reaction step of all the analysed three-prong events.

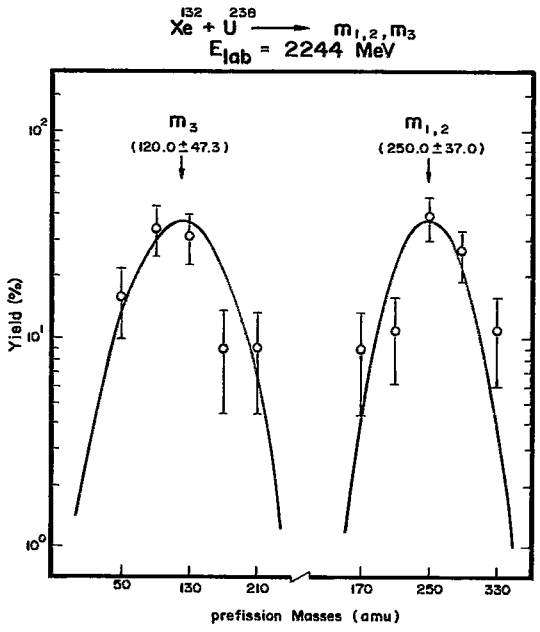

Fig. 4. Distribution of the masses in the first reaction step integrated over all angles and energies in the case of three-prong events. The fit on the right-hand side shows the pre-fission masses while the left-hand side shows the distribution of the masses which survived. Gaussians have been fitted with the arithmetic means and standard deviations.